bipy	2,2′-bipyridyl
diammac	6,13-dimethyl-1,4,8,11-tetraazacyclotetradecane-6,13-diamine
diamsar	3,6,10,13,16,19-hexaazabicyclo[6.6.6]eicosane-1,8-diamine
dien	bis(2-aminoethyl)amine
dipa	bis(2′-pyridyl)methanamine
dota	1,4,7,10-tetraazacyclododecane-*N*,*N*′,*N*″,*N*‴-tetraethanoate
dtne	1,2-bis(1,4,7-triaza-1-cyclononyl)ethane
eap	2′-pyridylethanamine
edda	ethane-1,2-diamine-*N*,*N*′-diethanoate
edta	ethane-1,2-diamine-*N*,*N*,*N*′,*N*′-tetraethanoate
en	ethane-1,2-diamine
gly	glycinate (aminoethanoate)
mn[13]aneN$_4$	12-methyl-12-nitro-1,4,7,10-tetraazacyclotridecane
mn[14]aneN$_4$	6-methyl-6-nitro-1,4,8-11-tetraazacyclotetradecane
mn[15]aneN$_4$	10-methyl-10-nitro-1,4,8,12-tetraazacyclopentadecane
mn[16]aneN$_4$	3-methyl-3-nitro-1,5,9,13-tetraazacyclohexadecane
mn[15.2]aneN$_4$	7-methyl-7-nitro-1,5,9,13-tetraazabicyclo-[11.2.2]heptadecane
mn[14]-aneN$_2$S$_2$	6-methyl-6-nitro-1,8-diaza-4,11-dithiacyclotetradecane
mnpala	5-methyl-5-nitro-2,5,8-trimethyl-5-nitro-3,7-diazanonanedioate
mnpbala	6-methyl-6-nitro-4,7-diazaundecanedioate
mnpgly	5-methyl-5-nitro-3,7-diazanonanedioate
[12]aneN$_4$	1,4,7,10-tetraazacyclododecane
[12]aneS$_4$	1,4,7,10-tetrathiacyclododecane
[13]aneS$_4$	1,4,7,11-tetrathiacyclotridecane
[14]aneS$_4$	1,4,8,11-tetrathiacyclotetradecane
[16]aneS$_4$	1,5,9,13-tetrathiacyclohexadecane
ndap	*N*,*N*′-bis(2′-pyridylmethyl)-2-methyl-2-nitropropane-1,3-diamine
phen	*o*-phenanthroline
ppm	*N*,*N*′-bis(2′-pyrrolidinylmethyl)propane-1,3-diamine
tach	*cis*,*cis*-cyclohexane-1,3,5-triamine
tacn	1,4,7-triazacyclononane
tacnta	1,4,7-triazacyclononane-*N*,*N*′,*N*″-triethanoate
terpy	2,2′,2″-terpyridyl
tn	propane-1,3-diamine

Contribution from the Institut für Anorganische Chemie, Universität Basel, Spitalstrasse 51, 4056 Basel, Switzerland, and the School of Chemistry, University of Sydney, 2006, Australia

Determination of Solution Structures of Binuclear Copper(II) Complexes

Paul V. Bernhardt,[1] Peter Comba,*[,1] Trevor W. Hambley,[2] Salah S. Massoud,[1,3] and Sandra Stebler[1]

Received January 23, 1992

A simple and efficient method for the determination of solution structures of weakly coupled binuclear copper(II) complexes is described. The technique involves the combination of molecular mechanics and EPR spectroscopy and has been applied to the binuclear copper(II) complexes of 5,5′-bis(3,7-dehydro-3,7-diazanonane-4,6-dione-1,9-diamine) (L^1), 5,5′-bis(3,7-diazanonane-1,9-diamine) (L^2), and 5-methyl-5-nitro-3,7-diazanonanedioate (L^3). The complexes $[Cu_2L^1]\cdot 10H_2O$ and $[Cu_2L^2](ClO_4)_4$ were also characterized by X-ray crystallography. $[Cu_2L^1]\cdot 10H_2O$: space group $P\bar{1}$; a = 7.669 (2), b = 8.757 (3), c = 10.596 (2) Å; α = 79.57 (3), β = 83.36 (2), γ = 89.17 (3)°. $[Cu_2L^2](ClO_4)_4$: space group $P3_221$; a = 13.671 (2), b = 13.671 (2), c = 13.929 (2) Å. There is excellent agreement between the X-ray crystal structures and the structures predicted by molecular mechanics and EPR spectroscopy. Electrochemical properties of the binuclear complexes are also reported.

Introduction

The pursuit of structures of large polynuclear coordination compounds, particularly those containing copper(II), has been largely motivated by a rather important role that such compounds play in bioinorganic systems.[4] Over the last decade or so, advances in protein X-ray crystallography have led to the solution of previously inaccessible structures of large biologically important molecules.[5] However, there are still problems associated with this technique, e.g., difficulties in obtaining X-ray quality crystals in addition to solution and precise refinement of the structure. Moreover, it should not be forgotten that the result of a crystal structure is not necessarily comparable with what one might find in solution. Solution techniques such as EXAFS have been applied to the determination of internuclear distances of large polynuclear complexes;[6] however, information such as the orientation of two coordination sites with respect to each other is beyond the scope of this method. NMR spectroscopy may give an insight to the connectivity and conformational geometry within large molecules such as metalloproteins;[7,8] however, a correct interpretation of the experimental spectrum is quite labor intensive. At this time, comparatively few solution structures of high molecular weight, biologically relevant molecules have been determined by NMR techniques alone.

Molecular mechanics calculations have been successfully applied to the determination of structures of small organic and coordination compounds.[9-12] The accuracy of such calculations generally leads to structures that are in agreement with those obtained from X-ray crystallographic studies, within experimental error. In most molecular mechanics studies of mononuclear complexes, a complete conformational analysis is necessary. However, when one considers high molecular weight systems, which generally possess greater conformational freedom, a somewhat restricted analysis must be adopted in order that the problem remains tractable. The relative strain energies of the isomers may give an indication of their abundance, but this alone is insufficient for a definite assignment of the solution structure. The same ambiguities are inherent to molecular mechanics calculations as to X-ray crystallography; i.e., there is still no guarantee that the solid-state and solution structures are the same. Therefore, additional spectroscopic evidence is necessary in order to corroborate predictions made by molecular mechanics calculations.

(1) Universität Basel.
(2) University of Sydney.
(3) Present address: University of Alexandria, Alexandria, Egypt.
(4) Solomon, E. I. In *Copper Proteins*; Spiro, T. G., Ed.; Wiley-Interscience: New York, 1981.
(5) Blundell, T. L.; Johnson, L. N. *Protein Crystallography*; Academic Press: New York, 1976.
(6) Spiro, T. G., Wollery, G. L.; Brown, J. M.; Powers, L.; Winkler, M. E.; Solomon, E. I. In *Copper Coordination Chemistry: Biochemical and Inorganic Perspectives*; Karlin, K. D., Zubieta, J., Eds.; Adenine Press: New York, 1983.
(7) Wüthrich, K. *Acc. Chem. Res.* **1989**, *22*, 36.
(8) Owens, C.; Drago, R. S.; Bertini, I.; Luchinat, C.; Banci, L. *J. Am. Chem. Soc.* **1986**, *108*, 3298.
(9) Allinger, N. L. *J. Am. Chem. Soc.* **1977**, *99*, 8127.
(10) Brubaker, G. R.; Johnson, C. D. *Coord. Chem. Rev.* **1984**, *53*, 1.
(11) Hancock, R. D. *Prog. Inorg. Chem.* **1989**, *36*, 187.
(12) Comba, P. *Coord. Chem. Rev.*, submitted.

0020-1669/92/1331-2644$03.00/0

Dicopper(II) complexes are well suited to study by EPR spectroscopy, since coupling of the nuclear and electronic spins of the two d^9 metal centers results in a spectrum quite different from that of a mononuclear analogue and rich in structural information regarding the separation and relative orientation of the two metal centers.[13] One can extract these structural parameters with a correct interpretation of the spectrum; however, this demands that computer simulation of the spectrum[14] be performed if a correct assignment of the EPR spectrum is to be obtained. Within the simulation procedure, there are a number of critical parameters that need to be determined other than those defining the orientation of the two metal centers. It is clear that such a large number of variables leads to numerous combinations of parameters that must be tried in pursuit of the "correct" solution. The serious implication of this is that there might be more than one combination of the above parameters that results in the same simulated spectrum. Another limitation of this method is that one can obtain no information regarding the conformation of the ligand backbone connecting the two metal centers.

The techniques of molecular mechanics and EPR spectroscopy may be combined in a complimentary sense in order to overcome their individual shortcomings. Simulation of the observed EPR spectrum using each molecular mechanics refined geometry as a starting point (from which there is ideally little deviation) leads to the solution structure of the complex. It must be remembered that the parameters defining the orientation of the two metal centers are meaningless if one has to fit the spectrum with absurd values of the spin Hamiltonian g and A parameters. Hence the final spin Hamiltonian parameters must be in accord with compounds of similar type. This methodology has been applied in the present case to the determination of solution structures of three binuclear copper(II) complexes of the ligands 5,5′-bis(3,7-dehydro-3,7-diazanonane-4,6-dione-1,9-diamine (L^1), 5,5′-bis-(3,7-diazanonane-1,9-diamine (L^2), and 5-methyl-5-nitro-3,7-diazanonanedioate (L^3). The dimeric copper(II) complex of L^3

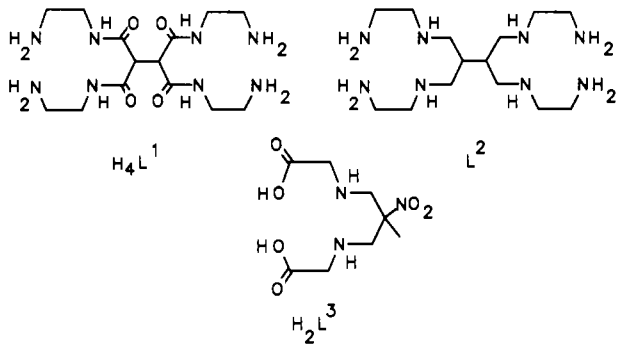

crystallizes as a monomer[15] and therefore cannot be characterized structurally in the solid state. The solution structure of this complex and of two additional dicopper(II) complexes of the ligands L^1 and L^2 have been determined by the combined techniques of molecular mechanics and EPR spectroscopy. The X-ray crystal structures of the dicopper(II) complexes of L^1 and L^2 are also reported herein, for comparison with the structures determined in solution.

Experimental Section

Syntheses. The complex (5-methyl-5-nitro-3,7-diazanonanedioate)-copper(II) ([CuL^3]) was prepared via a literature synthesis.[15] Tetraethyl 1,1,2,2-ethanetetracarboxylate was obtained from Aldrich Chemicals.

5,5′-Bis(3,7-diazanonane-4,6-dione-1,9-diamine) Dihydrate ($(H_4L^1)\cdot 2H_2O$). A solution of tetraethyl 1,1,2,2-ethanetetracarboxylate (15.0 g, 0.05 mol) in ethanol (50 mL) was treated with excess ethane-1,2-diamine (en; 80 mL). The reaction mixture was stirred at room temperature for 5 h. The resultant white precipitate was collected by filtration, washed with diethyl ether twice, and air-dried (17.5 g, 85%). Anal. Calcd for $C_{14}H_{34}N_8O_6$: C, 41.0; H, 8.4; N, 27.3. Found: C, 41.3; H, 8.2; N, 27.4. ^{13}C NMR (^2H_2O): 40.5, 42.3, 42.6, 169.7 ppm.

5,5′-Bis[(3,7-dehydro-3,7-diazanonane-4,6-dione-1,9-diamine)copper-(II)] Decahydrate ($[Cu_2L^1]\cdot 10H_2O$). To a solution of H_4L^1 (1.03 g, 2.5 mmol) in water (100 mL) was added copper(II) nitrate trihydrate (1.21 g, 5 mmol), and the pH of the mixture was raised to 7 with dilute sodium hydroxide solution. The resulting purple solution was passed through a 15 × 2 cm column of SP Sephadex C-25 cation-exchange resin (Na^+ form), which afforded separation of the neutral desired product from some cationic species. The eluate was evaporated to dryness under reduced pressure and redissolved in a minimum volume of water (λ_{max} 530 nm). Crystals suitable for X-ray study formed upon standing, were collected by filtration washed with diethyl ether, and air-dried (0.35 g, 21%). Anal. Calcd for $C_{14}H_{46}Cu_2N_8O_{14}$: C, 24.8; H, 6.8; N, 16.5. Found: C, 24.6; H, 7.0; N, 16.6.

5,5′-Bis[(3,7-diazanonane-1,9-diamine)copper(II)] Tetraperchlorate ($[Cu_2L^2](ClO_4)_4$). Under a nitrogen atmosphere, a suspension of finely powdered H_4L^1 (2.05 g, 5 mmol) in bis(2-methoxyethyl) ether (250 mL) was treated with BH_3·THF (150 mL, 1.0 M). The reaction mixture was stirred at 110 °C for 5 h, an additional 100 mL of reductant was added, and heating was continued for a further 16 h. The mixture was cooled to room temperature and the excess BH_3·THF was reacted by careful addition of methanol (ca. 80 mL) and then pyridine (20 mL). The suspension was filtered, and the filtrate was evaporated to dryness, treated with water (30 mL), HCl (15 mL, 10 M), and methanol (100 mL) and then again evaporated to dryness. The octahydrochloride salt of L^2 was found to be rather hygroscopic and was therefore stored in methanol. Purity of the ligand was found to be satisfactory from the ^{13}C NMR spectrum, which displayed resonances at 35.3, 36.2, 46.1 and 47.2 ppm. Some traces of ethane-1,2-diamine were found in the spectrum; however, further purification was deemed unnecessary for the purposes of the present study.

A methanolic solution of L^2·8HCL was diluted with water (100 mL) and neutralized with sodium hydroxide solution. To this was added 2 equiv of copper(II) nitrate. The pH of the solution was adjusted to 5, and the solution was filtered, diluted to 200 mL with water, and then charged on a 15 × 2 cm column of SP Sephadex C-25 cation-exchange resin. The column was washed with 0.2 M sodium perchlorate, which removed both uncomplexed copper(II) and $[Cu(en)_2]^{2+}$. The desired product was eluted with 0.4 M sodium perchlorate as a purple solution (λ_{max} 528 nm). The eluate was evaporated to 10 mL, methanol (60 mL) was added, and the resulting precipitate of sodium perchlorate was removed by filtration. Slow evaporation of the filtrate led to precipitation of the purple product, which was collected by filtration, washed with ethanol and then diethyl ether, and air-dried. The second crop afforded crystals suitable for X-ray work. Anal. Calcd for $C_{14}H_{38}Cl_4Cu_2N_8O_{16}$: C, 19.9; H, 4.5; N, 13.3; Cl, 16.8. Found: C, 20.2; H, 4.7; N, 13.0; Cl, 16.6.

Physical Methods. Electron paramagnetic resonance spectra were recorded as ca. 1-mmol solutions in DMF/H_2O (1:2) at 77 K on a Varian E9 X-band spectrometer employing diphenylpicrylhydrazyl as an external reference. Proton-decoupled ^{13}C nuclear magnetic resonance spectra were measured on a Varian Gemini 300 spectrometer, with chemical shifts being cited vs tetramethylsilane. Cyclic voltammetry and differential pulse polarography experiments were performed with a Metrohm E-612 controller and an E-611 detector. Glassy carbon working, platinum counter, and calomel reference electrodes were employed, and all solutions were ca. 1 mmol in complex, 0.1 M in $NaClO_4$ and were purged with nitrogen prior to measurement.

Molecular Mechanics. Calculations were performed with the strain minimization program MOMEC87.[16] The force field has been described elsewhere.[17] Some new parameters have been introduced in order to model the coordinated, deprotonated amide group in $[Cu_2L^1]$. The Cu–N(amide), C–N(amide), and C–O(amide) strain-free bond lengths (Å) and force constants (mdyn Å^{-1}) were respectively 1.920 and 0.60, 1.310 and 6.50, and 1.260 and 9.00. The remaining force field parameters (valence angle, torsion angle, and out-of-plane deformations) were identical to those employed for coordinated carboxylate groups.[17] In each binuclear complex, water molecules were refined in both axial sites; i.e., all copper(II) centers were modeled as six-coordinate complexes. Trial structures were produced with the graphics program SMILE,[18] and pictures of all molecules were obtained with the plotting program ORTEP.[19]

(13) Strictly speaking, one should only refer to the relative orientations of the g tensors in the x, y, and z directions, but since they generally coincide with the molecular axes in copper(II) complexes, and are more readily visualized, the symmetry axes will be referred to in this paper.
(14) Pilbrow, J. R.; Smith, T. D. *Coord. Chem. Rev.* **1974**, *13*, 173.
(15) Comba, P.; Hambley, T. W.; Lawrance, G. A.; Martin, L. L.; Renold, P.; Várnagy, K. *J. Chem. Soc., Dalton Trans.* **1991**, 277.
(16) Hambley, T. W. *MOMEC87, A Program for Strain Energy Minimization*; University of Sydney: Sydney, Australia, 1987.
(17) Bernhardt, P. V.; Comba, P. *Inorg. Chem.*, preceding paper in this issue.
(18) Eufri, D.; Sironi, A. *J. Mol. Graphics* **1989**, *7*, 8127.

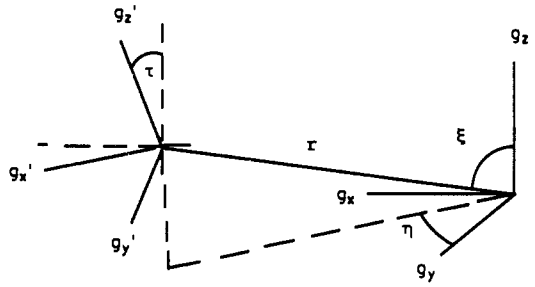

Figure 1. Definition of the parameters r, ξ, τ, and η.

Table I. Crystal Data for $[Cu_2L^1]\cdot 10H_2O$ and $[Cu_2L^2](ClO_4)_4$

	$[Cu_2L^1]\cdot 10H_2O$	$[Cu_2L^2](ClO_4)_4$
space group	$P\bar{1}$	$P3_221$
a, Å	7.669 (2)	13.671 (2)
b, Å	8.757 (3)	13.671 (2)
c, Å	10.596 (2)	13.929 (2)
α, deg	79.57 (3)	90.00
β, deg	83.36 (2)	90.00
γ, deg	89.17 (3)	120.00
V, Å^3	695.1	2254.50
fw	677.66	843.41
D_c, g/cm^3	1.660	1.863
empirical formula	$C_{14}H_{46}Cu_2N_8O_{14}$	$C_{14}H_{38}Cl_4Cu_2N_8O_{16}$
Z	1	3
abs coeff, cm^{-1}	15.75	36.02
transm coeff	0.924–0.714	0.821–0.675
temp, K	294	294
λ, Å	0.710 69	0.710 69
$R(F_o)$	0.032	0.037
$R_w(F_o)^a$	0.036	0.040

$^a w = g/(\sigma^2 F_o + kF_o^2)$.

EPR Simulations. The EPR spectra of all binuclear complexes were modeled with the simulation program DISSIM.[14] The most important input parameters to the program comprise the spin Hamiltonian parameters for each copper(II) center, the internuclear separation, r, and the three angles ξ, τ, and η defining the relative orientation of the **g** tensors of the two copper(II) moieties within the binuclear complex (Figure 1). The initial spin Hamiltonian parameters were taken from previously reported dicopper(II) complexes, and the trial set of angles defining the relative orientation of the two metal centers and the internuclear distances were obtained from the minimized strain energy geometries of each conformer. All of the above variables were modified until the simulated and experimental spectra were adequately matched. The mononuclear spectrum of $[CuL^3]$ was modeled with the program EPR50F.[20]

X-ray Crystal Structure Analyses. Lattice dimensions were determined by a least-squares fit to the setting parameters of 25 independent reflections, measured, and refined on an Enraf-Nonius CAD4 four-circle diffractometer employing graphite-monochromated Mo Kα radiation. Crystallographic data are summarized in Table I. Data reduction and application of Lorentz, polarization, and decomposition corrections were carried out using the Enraf-Nonius Structure Determination Package.[21]

The structures of $[Cu_2L^1]\cdot 10H_2O$ and $[Cu_2L^2](ClO_4)_4$ were solved by direct and Patterson methods, respectively, and refined by full-matrix least-squares analysis with SHELX76.[22] All non-hydrogen atoms, except the disordered O(21)–O(24), C(6), and C(7) atoms in the structure of $[Cu_2L^2](ClO_4)_4$, were refined with anisotropic thermal parameters. The disorder of C(6) and C(7) led to problems in locating H atoms associated with atoms N(3), C(6), C(7), and N(4), so the appropriate H atoms were fixed at estimated positions. All other H atoms were located and refined isotropically. The O(21)–O(24) atoms of one pair of symmetry-related perchlorate anions were disordered over three sites with approximately equal occupancies and were also refined with isotropic thermal parameters. Scattering factors and anomalous dispersion coefficients for Cu were taken from the literature,[23] whereas the remaining values were supplied in SHELX76 and plots were produced with ORTEP.[19] Non-hydrogen atom coordinates are listed in Tables II and III, and listings of H atom coordinates, thermal parameters, observed and calculated structure factor amplitudes and complete crystal data have been deposited as supplementary material.

Table II. Positional Parameters ($\times 10^4$) for $[Cu_2L^1]\cdot 10H_2O$

Cu(1)	1961 (1)	−179 (1)	2863 (1)
N(1)	1520 (4)	1181 (3)	1181 (3)
N(2)	3301 (3)	1597 (3)	3117 (2)
N(3)	2021 (3)	−1322 (3)	4608 (2)
N(4)	163 (4)	−1797 (4)	2737 (3)
C(1)	2855 (5)	2446 (4)	898 (3)
C(2)	3083 (5)	2983 (3)	2147 (3)
C(3)	3783 (3)	1813 (3)	4217 (3)
C(4)	4118 (3)	392 (3)	5225 (3)
C(5)	2658 (3)	−848 (3)	5558 (3)
C(6)	736 (4)	−2595 (4)	4966 (3)
C(7)	382 (5)	−3146 (4)	3751 (4)
O(1)	4051 (3)	3126 (2)	4497 (2)
O(2)	2220 (3)	−1368 (2)	6748 (2)
OW(1)	5504 (4)	5917 (3)	3248 (3)
OW(2)	4080 (4)	8318 (4)	1662 (4)
OW(3)	1806 (4)	−4358 (4)	8136 (3)
OW(4)	7109 (4)	245 (5)	1114 (3)
OW(5)	8877 (5)	3596 (4)	9366 (3)

Table III. Positional Parameters ($\times 10^4$) for $[Cu_2L^2](ClO_4)_4$[a]

Cu(1)	−3453 (1)	−199 (1)	−500 (1)
N(1)	8103 (4)	261 (5)	−7 (4)
N(2)	7322 (3)	1066 (3)	−1445 (3)
N(3)	5083 (3)	−810 (4)	−1219 (3)
N(4)	5706 (5)	−1490 (5)	403 (4)
C(1)	8892 (5)	946 (7)	−783 (5)
C(2)	8522 (5)	1740 (5)	−1163 (6)
C(3)	7182 (5)	660 (5)	−2444 (4)
C(4)	5957 (4)	111 (5)	−2782 (3)
C(5)	5179 (5)	−983 (5)	−2247 (4)
C(6)	4299 (11)	−2033 (11)	−839 (9)
C(7)	4450 (11)	−1942 (10)	227 (9)
C(6′)	4179 (10)	−1713 (10)	−644 (9)
C(7′)	4652 (12)	−2329 (12)	−192 (11)
Cl(1)	5540 (1)	1430 (1)	435 (1)
O(11)	6364 (4)	1123 (5)	676 (4)
O(12)	5608 (5)	2277 (5)	1045 (5)
O(13)	4449 (4)	470 (4)	498 (5)
O(14)	5770 (6)	1847 (5)	−518 (5)
Cl(2)	2448 (2)	−182 (1)	5076 (2)
O(21)	2275 (17)	730 (15)	5226 (11)
O(22)	1779 (17)	−759 (15)	4170 (13)
O(23)	1846 (14)	8809 (14)	5541 (13)
O(24)	3631 (17)	335 (17)	5185 (16)
O(21′)	1806 (18)	−3 (20)	5864 (18)
O(22′)	3166 (20)	903 (20)	4753 (17)
O(23′)	2353 (30)	9485 (26)	4069 (21)
O(24′)	2938 (28)	9251 (30)	5620 (21)
O(21″)	1800 (21)	322 (21)	5478 (19)
O(22″)	1729 (21)	8787 (22)	4853 (20)
O(23″)	3454 (21)	590 (21)	4605 (17)
O(24″)	3266 (33)	9844 (37)	5935 (27)
O(25)	1559 (43)	−268 (41)	5073 (34)

[a] Primes indicate disordered atoms.

Results and Discussion

Syntheses and Electronic Properties. Syntheses of the ligands H_4L^1 and L^2 and their dicopper(II) complexes were relatively straightforward. In contrast to the preparation of a macrocyclic analogue of L^1 under conditions of high dilution,[24] it was possible to react the parent ester with a large excess of ethane-1,2-diamine (en) in order to avoid intramolecular cyclization. A rather surprising observation was the instability of H_4L^1 in aqueous solution.

(19) Johnson, C. K. *ORTEP, A Thermal Ellipsoid Plotting Program*; Oak Ridge National Laboratory, Oak Ridge, TN, 1965.
(20) Martinelli, R. A.; Hanson, G. R.; Thompson, J. S.; Holmquist, B.; Pilbrow, J. R.; Auld, D. S.; Vallee, B. L. *Biochemistry* **1989**, *28*, 2251.
(21) Enraf-Nonius Structure Determination Package, Enraf-Nonius, Delft, The Netherlands, 1985.
(22) Sheldrick, G. M. *SHELX76, A Program for X-ray Crystal Structure Determination*; University of Cambridge: Cambridge, UK, 1976.
(23) Cromer, D. T.; Waber, J. T. *International Tables for X-ray Crystallography*; Kynoch Press: Birmingham, UK, 1974; Vol. IV.
(24) Fabbrizzi, L.; Forlini, F.; Perotti, A.; Seghi, B. *Inorg. Chem.* **1984**, *23*, 807.

The ligand underwent complete hydrolysis in neutral aqueous solution at room temperature within a few hours. This unusually rapid hydrolysis was presumably promoted by the primary amine groups via an intramolecular base-catalyzed pathway. No such reactivity was reported for the 14-membered bismacrocyclic analogue of H_4L^1.[24] The complex $[Cu_2L^1]$ was more stable than the parent ligand; however, it too underwent hydrolysis to $[Cu(en)_2]^{2+}$ over a period of a couple weeks. Nevertheless, the relatively low solubility of $[Cu_2L^1]$ facilitated its rapid precipitation from aqueous solution without hydrolysis of the ligand occurring. Reduction of H_4L^1 to its amine relative L^2 proved to be rather poor yielding. Reaction with $LiAlH_4$ resulted in destruction of the amide with no amine being formed. This necessitated the employment of BH_3 as a reductant and a longer reaction time. The yield, however, was still rather low (an observation noted by others concerned with similar systems[25]), and a large amount of en was detected as a reaction product. There are two likely explanations for the poor yield of amine. The rather sluggish kinetics inherent to borane reductions of amides might have dictated that very little of the desired amine was produced during the 24-h reaction time and that a longer reaction time was necessary. The other explanation is that cleavage of the amide occurred during BH_3 reduction in a manner akin to that found for the $LiAlH_4$ reduction. As mentioned above, the instability of the amide in aqueous solution would result in complete hydrolysis of any unreacted H_4L^1 to en so either of the above explanations would lead to the same observation. Optimized conditions for the reactions were not pursued in the present study since large quantities of the amide H_4L^1 could be produced and the amount of $[Cu_2L^2]^{4+}$ that was needed for spectroscopic studies was minimal.

The electronic spectra of $[Cu_2L^1]$ and $[Cu_2L^2]^{4+}$ did not differ greatly from those of mononuclear analogues, both being consistent with Cu(II) in a plane of four N donors with weak axial interactions from solvent molecules. The aqueous electrochemistry of $[Cu_2L^1]$ and $[Cu_2L^2]^{4+}$ revealed markedly different behavior going from the amide complex to its amine relative. Complete oxidation of $[Cu_2L^1]$ to the trivalent state was achieved in aqueous solution via consecutive one-electron processes at $E_{1/2}$ of +0.84 and +1.03 V vs SHE, which is comparable with the polarographic behavior of bismacrocyclic analogues.[24] Although strictly irreversible, substantial reduction waves were found in the cyclic voltammogram ($i_c/i_a \sim 0.8$ at 100 mV/s scan rate). The large separation of the two $Cu^{III/II}$ couples is indicative of a significant internuclear electrostatic interaction; i.e., the second electron is more difficult to remove than the first due to the influence of the adjacent Cu^{III} center. No oxidation processes for $[Cu_2L^2]^{4+}$ were identified, which is not surprising since the $Cu^{III/II}$ redox couples of tetraaminecopper(II) complexes invariably lie outside the potential limits set by neutral aqueous solution. Individual $Cu^{II/I}$ waves of $[Cu_2L^2]^{4+}$ were unable to be resolved but instead a single wave was detected at $E_{1/2}$ of −0.58 V vs SHE, which is ca. 200 mV more negative than that observed for mononuclear relatives.[26] No reduction processes for $[Cu_2L^1]$ were evident within the experimental potential range (i.e., +1.2 to −1.2 V vs SHE).

Structural Characterization. (a) $[Cu_2L^1]$. Three distinct geometries of this complex are shown in Figure 2. There is conformational freedom in the five-membered chelate rings; however, molecular mechanics calculations reveal that the energy difference between the λ and δ conformers is small by comparison with relative strain energies of the three conformers shown in Figure 2. More importantly, the conformational changes do not perturb the internuclear separations or the angles defining the orientation of the two metal centers, so their exact positions were not relevant to the present study. The total strain energies, internuclear separations, and angles ξ, τ, and η for the three isomers are given in Table IV.

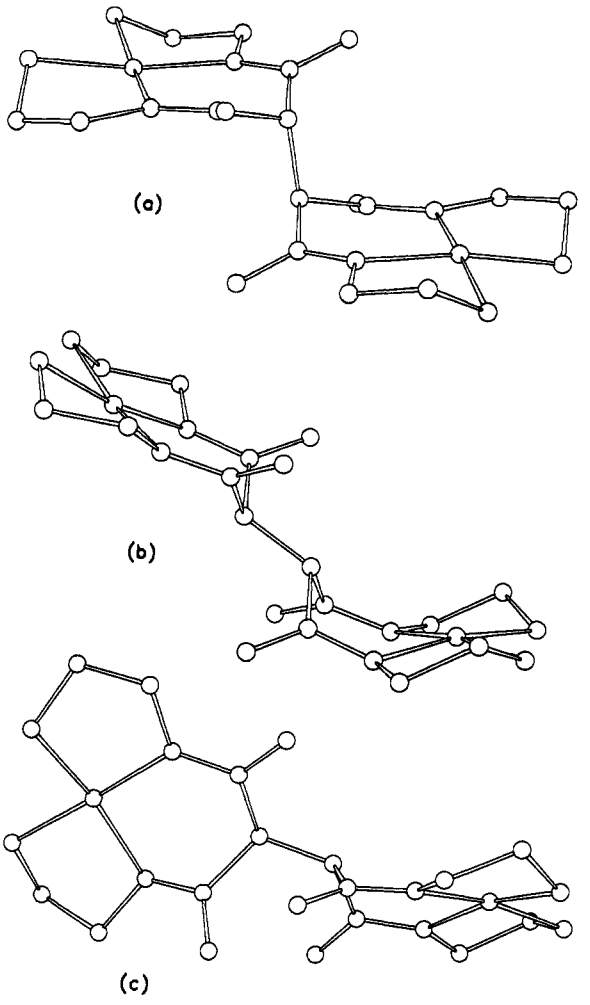

Figure 2. Strain energy minimized isomers of $[Cu_2L^1]$.

Table IV. Geometric Parameters (Figure 1) of the Strain Energy Minimized Structures (Figure 2), Refined Solution Structure, and X-Ray Crystal Structure of $[Cu_2L^1]\cdot 10H_2O$

structure type	r (Å)	ξ (deg)	τ (deg)	η (deg)	strain energy (kJ/mol)
a	7.2	75	0	0	45.10
b	7.4	48	42	0	46.75
c	7.8	68	35	4	53.75
solution	6.7	67	0	0	
crystal	6.9	70	0	0	

Inspection of the relative minimized strain energies for the three isomers (Table IV) indicated that structure a in Figure 2 was the most likely one to be observed experimentally. Nevertheless, it was found that a slight modification of the values r and ξ was necessary in order to fit the simulated EPR spectrum of $[Cu_2L^1]$ to the experimental spectrum (Figure 3). The values of r, ξ, τ, and η determined from the EPR spectrum are given in Table IV. The g values ($g_\parallel$ 2.20, $g_\perp$ 2.05) are not unusual, and the $A_\parallel$ values for both metal centers (90×10^{-4} cm^{-1}) are approximately half of those characteristic of mononuclear copper(II) complexes in a tetragonally distorted octahedral environment. The deviation of A values from those found in mononuclear complexes is a common[27-29] but poorly understood observation in the EPR spectra of binuclear copper(II) complexes. The $A_\perp$ values (25×10^{-4} cm^{-1}) are also typical of complexes such as these.

(25) Fabbrizzi, L.; Montagna, L.; Poggi, A.; Kaden, T. A.; Siegfried, L. C. *J. Chem. Soc., Dalton Trans.* **1987**, 2631.
(26) Bernhardt, P. V.; Lawrance, G. A.; Skelton, B. W.; White, A. H. *Aust. J. Chem.* **1990**, *43*, 399.
(27) Boas, J. F.; Dunhill, R. H.; Pilbrow, J. R.; Srivastava, R. C.; Smith, T. D. *J. Chem. Soc. A* **1969**, 94.
(28) Chasteen, N. D.; Belford, R. L. *Inorg. Chem.* **1970**, *9*, 169.
(29) Bernhardt, P. V.; Comba, P.; Gahan, L. R.; Lawrance, G. A. *Aust. J. Chem.* **1990**, *43*, 2035.

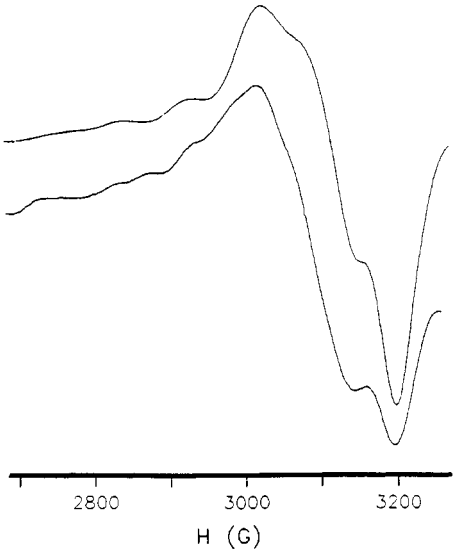

Figure 3. Simulated (top) and experimental frozen solution EPR spectra (77 K) of $[Cu_2L^1]$.

Table V. Bond Lengths (Å) for $[Cu_2L^1]\cdot 10H_2O$ and $[Cu_2L^2](ClO_4)_4$

	$[Cu_2L^1]\cdot 10H_2O$		
N(1)–Cu(1)	2.017 (3)	C(6)–N(3)	1.466 (3)
N(2)–Cu(1)	1.953 (2)	C(7)–N(4)	1.468 (5)
N(3)–Cu(1)	1.942 (2)	C(2)–C(1)	1.512 (5)
N(4)–Cu(1)	2.023 (3)	C(4)–C(3)	1.526 (4)
OW(2)–Cu(1)	2.460 (3)	C(5)–C(4)	1.538 (3)
C(1)–N(1)	1.486 (4)	C(4)–C(4)	1.572 (5)
C(2)–N(2)	1.462 (4)	C(7)–C(6)	1.507 (5)
C(3)–N(2)	1.309 (4)	O(1)–C(3)	1.263 (3)
C(5)–N(3)	1.302 (4)	O(2)–C(5)	1.269 (3)
	$[Cu_2L^2](ClO_4)_4$		
N(1)–Cu(1)	2.015 (5)	C(4)–C(4)	1.56 (1)
N(2)–Cu(1)	2.004 (4)	C(7)–C(6)	1.59 (2)
N(3)–Cu(1)	2.007 (4)	C(7′)–C(6′)	1.44 (2)
N(4)–Cu(1)	1.998 (5)	O(11)–Cl(1)	1.425 (5)
O(11)–Cu(1)	2.543 (7)	O(12)–Cl(1)	1.402 (5)
C(1)–N(1)	1.483 (8)	O(13)–Cl(1)	1.413 (5)
C(2)–N(2)	1.478 (7)	O(14)–Cl(1)	1.419 (6)
C(3)–N(2)	1.474 (7)	O(21)–Cl(2)	1.40 (2)
C(5)–N(3)	1.469 (8)	O(22)–Cl(2)	1.53 (2)
C(6)–N(3)	1.56 (1)	O(23)–Cl(2)	1.37 (2)
C(6′)–N(3)	1.47 (1)	O(24)–Cl(2)	1.41 (2)
C(7)–N(4)	1.53 (1)	O(21′)–Cl(2)	1.50 (2)
C(7′)–N(4)	1.56 (2)	O(22′)–Cl(2)	1.38 (2)
C(2)–C(1)	1.50 (1)	O(23′)–Cl(2)	1.46 (3)
C(4)–C(3)	1.527 (7)	O(24′)–Cl(2)	1.46 (3)
C(5)–C(4)	1.528 (8)		

The X-ray crystal structure of $[Cu_2L^1]\cdot 10H_2O$ found the complex to be located on a center of symmetry with five pairs of symmetry-related water molecules being situated at general positions.[30] An ORTEP drawing of the molecule appears in Figure 4, and the similarity between the geometry and that depicted in Figure 2a is apparent. The copper(II) environment is five-coordinate square pyramidal with the metal center being displaced 0.183 Å out of the least-squares plane of four N donors toward the apical aqua ligand. There are numerous hydrogen-bonding interactions between adjacent water molecules in addition to amine hydrogen–water contacts. The interatomic distances and angles are given in Tables V and VI. The intramolecular Cu–Cu distance is 6.9 Å, which is comparable with values of 7.2 Å predicted by molecular mechanics calculations and 6.7 Å obtained from the simulated EPR spectrum. The crystallographically determined angles ξ, τ, and η are in good agreement with those derived from

(30) Another group has independently solved the X-ray crystal structure of $[Cu_2L^1]\cdot 10H_2O$: Luo, Q.; Zhu, S.; Shen, M. Abstracts, XVI International Symposium on Macrocyclic Chemistry, Sheffield, UK, 1991; Poster P9.

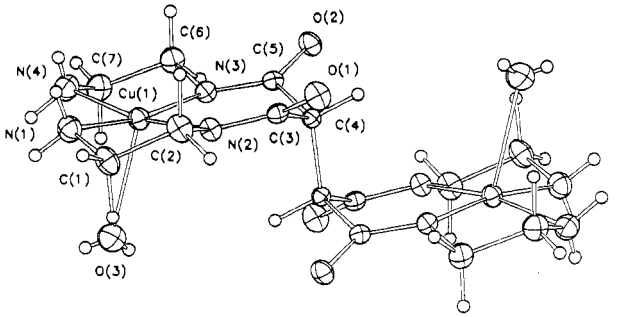

Figure 4. ORTEP plot of $[Cu_2L^1]$ (axial aqua ligands included).

Table VI. Bond Angles (deg) for $[Cu_2L^1]\cdot 10H_2O$ and $[Cu_2L^2](ClO_4)_4$

	$[Cu_2L^1]\cdot 10H_2O$		
N(2)–Cu(1)–N(1)	84.6 (1)	N(3)–Cu(1)–N(1)	170.0 (1)
N(3)–Cu(1)–N(2)	95.0 (1)	N(4)–Cu(1)–N(1)	94.0 (1)
N(4)–Cu(1)–N(2)	168.8 (1)	N(4)–Cu(1)–N(3)	84.4 (1)
OW(2)–Cu(1)–N(1)	89.4 (1)	OW(2)–Cu(1)–N(2)	104.8 (1)
OW(2)–Cu(1)–N(3)	100.3 (1)	OW(2)–Cu(1)–N(4)	86.3 (1)
C(1)–N(1)–Cu(1)	107.5 (2)	C(2)–N(2)–Cu(1)	112.6 (2)
C(3)–N(2)–Cu(1)	125.6 (2)	C(3)–N(2)–C(2)	117.0 (2)
C(5)–N(3)–Cu(1)	127.2 (2)	C(6)–N(3)–Cu(1)	113.5 (2)
C(6)–N(3)–C(5)	116.3 (2)	C(7)–N(4)–Cu(1)	107.6 (2)
C(2)–C(1)–N(1)	108.2 (3)	C(1)–C(2)–N(2)	107.4 (2)
C(4)–C(3)–N(2)	118.5 (2)	O(1)–C(3)–N(2)	124.6 (3)
O(1)–C(3)–C(4)	116.9 (3)	C(5)–C(4)–C(3)	116.3 (2)
C(4)–C(5)–N(3)	118.0 (2)	O(2)–C(5)–N(3)	125.4 (2)
O(2)–C(5)–C(4)	116.6 (2)	C(7)–C(6)–N(3)	108.2 (3)
C(6)–C(7)–N(4)	109.3 (3)		
	$[Cu_2L^2](ClO_4)_4$		
N(2)–Cu(1)–N(1)	86.2 (2)	N(3)–Cu(1)–N(1)	167.8 (2)
N(3)–Cu(1)–N(2)	91.1 (2)	N(4)–Cu(1)–N(1)	96.4 (2)
N(4)–Cu(1)–N(2)	177.3 (2)	N(4)–Cu(1)–N(3)	86.2 (2)
C(1)–N(1)–Cu(1)	105.7 (4)	C(2)–N(2)–Cu(1)	107.9 (4)
C(3)–N(2)–Cu(1)	112.5 (3)	C(3)–N(2)–C(2)	112.4 (5)
C(5)–N(3)–Cu(1)	113.7 (4)	C(6)–N(3)–Cu(1)	106.5 (5)
C(6)–N(3)–C(5)	103.1 (6)	C(6′)–N(3)–Cu(1)	108.8 (5)
C(6′)–N(3)–C(5)	120.0 (6)	C(7)–N(4)–Cu(1)	106.8 (5)
C(7′)–N(4)–Cu(1)	103.1 (6)	C(2)–C(1)–N(1)	108.2 (6)
C(1)–C(2)–N(2)	108.2 (5)	C(4)–C(3)–N(2)	112.4 (4)
C(5)–C(4)–C(3)	112.7 (4)	C(4)–C(5)–N(3)	113.1 (5)
C(7)–C(6)–N(3)	104.8 (9)	C(6)–C(7)–N(4)	105.9 (9)
O(12)–Cl(1)–O(11)	111.5 (3)	O(13)–Cl(1)–O(11)	109.5 (4)
O(13)–Cl(1)–O(12)	109.4 (3)	O(14)–Cl(1)–O(11)	106.9 (3)
O(14)–Cl(1)–O(12)	109.0 (4)	O(14)–Cl(1)–O(13)	110.5 (4)
O(22)–Cl(2)–O(21)	105.1 (9)	O(23)–Cl(2)–O(21)	123 (1)
O(23)–Cl(2)–O(22)	88 (1)	O(24)–Cl(2)–O(21)	101 (1)
O(24)–Cl(2)–O(22)	126 (1)	O(24)–Cl(2)–O(23)	114 (1)
O(23′)–Cl(2)–O(21′)	141 (2)	O(23′)–Cl(2)–O(22′)	85 (2)
O(24′)–Cl(2)–O(21′)	99 (2)	O(24′)–Cl(2)–O(22′)	118 (2)
O(24′)–Cl(2)–O(23′)	109 (2)		

Table VII. Strain Energy Minimized Geometries of the Four Conformers (Figure 5), Refined Solution Structure, and X-ray Crystal Structure of $[Cu_2L^2](ClO_4)_4$

structure type	r (Å)	ξ (deg)	τ (deg)	η (deg)	strain energy (kJ/mol)
a	8.0	70	75	29	46.80
b	8.3	81	14	0	56.56
c	8.0	61	62	0	78.38
d	7.1	61	36	0	49.13
solution	8.0	70	75	29	
crystal	7.9	58	80	33	

the molecular mechanics/EPR simulation analysis, and these values are also presented in Table IV.

(b) $[Cu_2L^2](ClO_4)_4$. The absence of the relatively bulky carbonyl oxygens in $[Cu_2L^2]^{4+}$ compared with $[Cu_2L^1]$ allows a greater rotational freedom in the amine complex, and four distinct geometries are possible (Figure 5). Conformational freedom of the five-membered chelate rings has been neglected for reasons discussed above, and the sterically favored chair conformers have

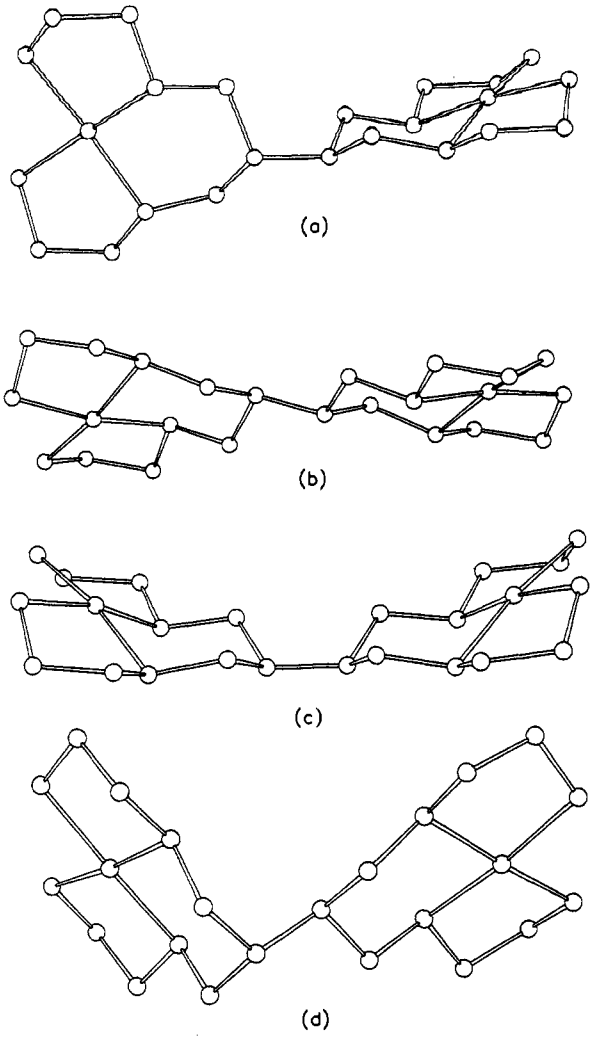

Figure 5. Strain energy minimized isomers of $[Cu_2L^2]^{4+}$.

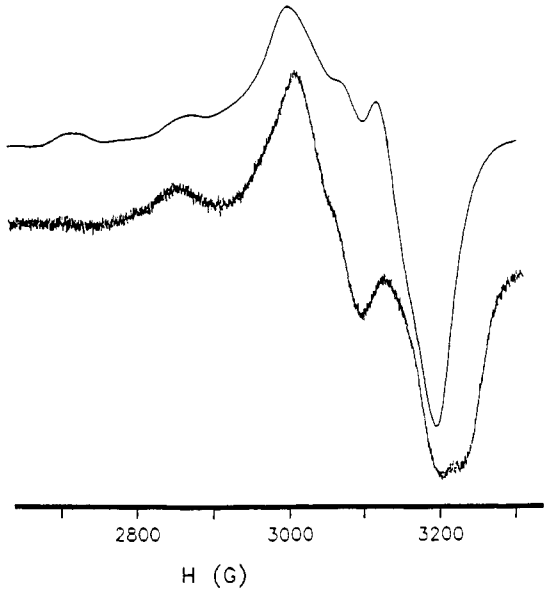

Figure 6. Simulated (top) and experimental frozen solution EPR spectra (77 K) of $[Cu_2L^2]^{4+}$.

been assumed for the six-membered chelate rings. The strain energies and r, ξ, τ, and η values for the four isomers are given in Table VII.

The EPR spectrum of $[Cu_2L^2](ClO_4)_4$ at 77 K is shown in Figure 6. Although the spectrum is rather poorly resolved, it was apparent that isomer a in Figure 5 was the geometry matching

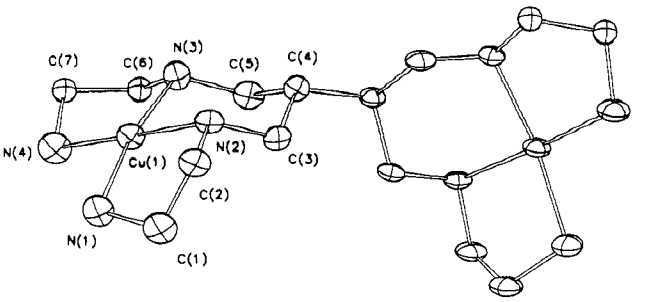

Figure 7. ORTEP view of the $[Cu_2L^2]^{4+}$ cation (hydrogen atoms omitted for clarity).

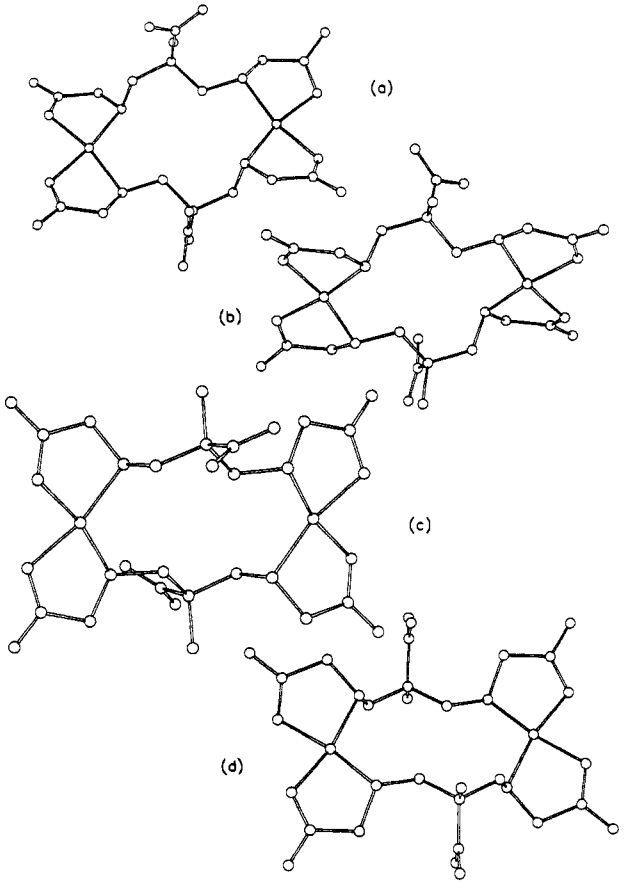

Figure 8. Strain energy minimized isomers of $[Cu_2L^3{}_2]$.

the EPR spectrum, which again was in agreement with what one would predict considering strain energies alone. Note that the two CuN_4 planes are not parallel and the Cu–Cu separation is 8.0 Å, in contrast to that found in the parent amide complex (6.7 Å). The spin Hamiltonian values ($g_\parallel$ 2.28, $g_\perp$ 2.055, $A_\parallel$ 155 × 10^{-4} cm^{-1}, $A_\perp$ 40 × 10^{-4} cm^{-1}) display trends similar to those shown by the $[Cu_2L^1]$ parameters.

The X-ray crystal structure of $[Cu_2L^2](ClO_4)_4$ found the complex cation to be situated on a twofold axis with perchlorate anions on general sites. The Cu environment comprises the four N donors and an axially ligating perchlorate anion. There is a slight tetrahedral distortion of the CuN_4 plane. A view of the $[Cu_2L^2]^{4+}$ cation is given in Figure 7. For clarity, the H atoms and the ligating perchlorate anions have been omitted, and one of the two conformers of the disordered five-membered chelate rings has been shown. A list of bond lengths and angles is given in Tables V and VI, and the appropriate crystallographic values of r, ξ, τ, and η are presented in Table VII for comparison with those obtained from the molecular mechanics/EPR simulation analysis. Examination of Table VII and comparison of Figures 5a and 7 illustrate that X-ray crystallography and the combination of molecular mechanics and EPR spectroscopy have led to the same structure in solution as in the solid state.

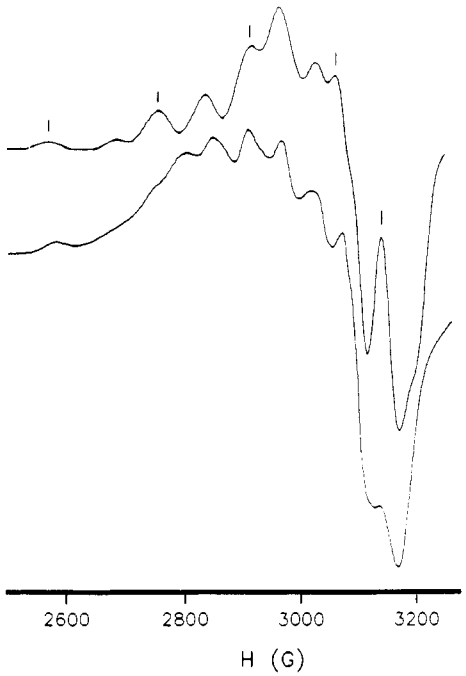

Figure 9. Simulated (top) and experimental frozen solution EPR spectra (77 K) of $[Cu_2L^3_2]/[CuL^3]$. Monomer contributions to the overall spectrum indicated by bars.

(c) $[Cu_2L^3_2]$. The dimeric copper(II) complex of the glycine derivative L^3 is a rather interesting example of a complex that exists as a mixture of $[CuL^3]$ and $[Cu_2L^3_2]$ in solution but which crystallizes as a monomer, as shown by X-ray crystallography.[15] The solution EPR spectrum of the complex exhibits peaks characteristic of both a monomer and a dimer (Figure 9); therefore it was necessary to model the spectrum of the monomeric complex before the spectrum of the dimer could be interpreted. This was a relatively simple procedure since the g and A values for mononuclear complexes of substituted relatives of L^3 are readily available.[15,31]

The complex $[Cu_2L^3_2]$ possesses a considerable amount of conformational freedom, so a slightly different approach was adopted in order to obtain the solution structure. A simulation of the EPR spectrum was attempted prior to molecular mechanics calculations being performed. Although the fit between the experimental and the simulated spectrum at this early stage was not satisfactory, it was apparent that the internuclear separation was in the range 6.5–7.0 Å, and the angles ξ, τ, and η were approximately 70°, 0°, and 0°, respectively. An internuclear distance of 6.8 Å and the above values of ξ, τ, and η were adopted so as to define the positions of the two metal centers; then the two ligand backbones were constructed around the metal ions. This provided a trial structure for the molecular mechanics calculations which was refined in the absence of the pendent methyl and nitro groups. It was immediately apparent that other N-based isomers of $[Cu_2L^3_2]$ were not consistent with the above angles and distances, and hence these isomers were not considered further. The pendant groups were then attached in the four possible combinations which result in the four isomers shown in Figure 8. Minimization of the strain energy of the four isomers gave very similar geometries, each with total strain energies of comparable magnitude (Table VIII).

The contribution of the monomer to the overall experimental spectrum is indicated in Figure 9. The orientations of the two copper(II) centers in $[Cu_2L^3_2]$ derived from the molecular mechanics predictions of the most stable conformer (Figure 8a) did not require major modification in order to simulate the contribution of the dimer to the EPR spectrum. The simulated sum of the contributions of $[CuL^3]$ and $[Cu_2L^3_2]$ to the overall EPR spectrum is also shown in Figure 9 and the values of r, ξ, τ, and η are given in Table VIII. The spin Hamiltonian parameters ($g_\parallel$ 2.25, $g_\perp$ 2.07, $A_\parallel$ 80 × 10^{-4} cm^{-1}, $A_\perp$ 35 × 10^{-4} cm^{-1}) are not unusual for binuclear copper(II) complexes, as discussed above.

Table VIII. Strain Energy Minimized Geometries of the Four Conformers (Figure 8) and Refined Solution Structure of $[Cu_2L^3_2]$

structure type	r (Å)	ξ (deg)	τ (deg)	η (deg)	strain energy (kJ/mol)
a	6.7	67	5	0	77.87
b	6.7	68	4	4	66.28
c	6.7	69	4	2	68.04
d	6.7	68	0	0	72.03
solution	6.7	73	5	6	

It is interesting to note that replacement of the pendent nitro group in $[CuL^3]$ with a primary amine leads to the same experimental spectrum as seen in Figure 9, as does methyl substitution on one α-carbon of L^3.[31] Any greater degree of substitution on the framework of L^3 leads exclusively to monomeric complexes. Close inspection of the strain energy minimized geometries of $[Cu_2L^3_2]$ (Figure 8) reveals that the α-carbon of but one amino acid residue of L^3 may be substituted in order to maintain the geometry shown in Figure 8. If more substituents are introduced, then severe steric crowding is the result and the dimeric structure becomes unstable. It appears that this is the driving force behind the observation of dimeric complexes of L^3 and its close relatives, in contrast to monomeric complexes of the more highly substituted ligands. In passing it is worth noting that the minimized strain energy of $[Cu_2L^3_2]$ (66.3 kJ/mol) is indeed less than twice the strain energy of $[CuL^3]$ (44.1 kJ/mol), suggesting that the observation of the dimer in solution is a result of thermodynamics, whereas the isolation of $[CuL^3]$ in the solid state is essentially a matter of preferential crystallization of the monomer over the dimer.

Conclusions

It has been shown that the combination of molecular mechanics and EPR spectral simulation is an effective method in the determination of the solution structure of dicopper(II) complexes. The calculated structures of $[Cu_2L^1]$ and $[Cu_2L^2]^{4+}$ were both reproduced by X-ray crystal structure, which is presently the only viable test of a predictive structural method concerned with complexes of this size. It should be remembered that, separately, molecular mechanics calculations of transition metal complexes and the simulation of EPR spectra of binuclear complexes have been in existence for some time. However, the combination of EPR simulation and molecular mechanics in the present study allows one to utilize the powers of both techniques. This results in a greater degree of certainty in the final results being representative of the experimental situation than would otherwise be found if either method was used in isolation. In the absence of molecular mechanics, approximately twice the number of EPR simulation variables must be determined by trial and error and little guarantee is given that they represent "the" correct combination of parameters. In all three cases presented herein, the conformer exhibiting the lowest strain energy was found to be the geometry representing the solution structure; thus additional support for the assignment of a given structure may be found in the relative stabilities of the complexes. In the two examples where characterization in the solid state was possible, the calculated solution structure and the X-ray crystal structure were not significantly different, although this need not be necessarily so as pointed out above. Any discrepancies may reflect shortcomings in the molecular mechanics force field and the EPR simulation routine, or they may define genuine differences between the solution and the solid-state structures. The technique described herein is not restricted to dicopper(II) complexes alone, but may be extended to hetero- and homobinuclear complexes of metal ions each with a single unpaired electron, e.g., low-spin Fe(III), V(IV), and Mo(V). If the experimental procedures are feasible, substitution of EPR-silent metal centers in biologically important binuclear systems by metal ions such as copper(II) has the potential to expand the use of the present method to the elucidation

(31) Balla, J.; Bernhardt, P. V.; Buglyo, P.; Comba, P.; Hambley, T. W.; Schmidlin, R.; Stebler, S.; Várnagy, K., manuscript in preparation.

of solution structures of a wide variety of binuclear complexes.

Acknowledgment. We gratefully acknowledge financial support of the Swiss National Science Foundation (Grant 20-28522.90). S.S.M. is grateful to the University of Alexandria for granting him a leave of absence.

Registry No. H_4L^1, 141376-66-1; Cu_2L^1, 141376-71-8; $[Cu_2L^1]\cdot 10H_2O$, 141376-68-3; $[Cu_2L^1]^+$, 141376-72-9; $[Cu_2L^1]^{2+}$, 141376-73-0; L^2, 141376-67-2; $[Cu_2L^2](ClO_4)_4$, 141376-70-7; CuL^3, 133370-41-9; $C_2L^3_2$, 141376-74-1; tetraethyl 1,1,2,2-ethanetetracarboxylate, 632-56-4; ethane-1,2-diamine, 107-15-3.

Supplementary Material Available: Listings of H atom coordinates, thermal parameters, and crystal data for $[Cu_2L^1]\cdot 10H_2O$ and $[Cu_2L^2](ClO_4)_4$ (4 pages); tables of observed and calculated structure factors for the abovementioned compounds (24 pages). Ordering information is given on any current masthead page.

Contribution from the Chemistry Department,
Case Western Reserve University, Cleveland, Ohio 44106

Why the Addition of CO Leads to Acyl Decarbonylation in a Supported Rh Dimer Complex

S.-F. Jen and Alfred B. Anderson*

Received July 30, 1991

Iwasawa and co-workers have recently found that the addition of CO to a Rh dimer complex with an acyl ligand (bound to a silica support) causes decarbonylation accompanied by Rh–Rh bond breaking. Ordinarily decarbonylation occurs in the absence of CO pressure. On the basis of ASED–MO calculations, we find that the driving force for decarbonylation is the stability of the nearly square-planar d^8 Rh that is formed:

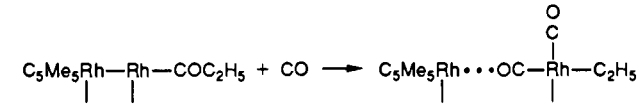

Here the Rh–Rh bond has been cleaved and a CO of the complex on the right forms a weak σ-donation bond with the Rh on the left.

Introduction

It has been known for a while that rhodium monomer complexes have good effectiveness for the hydroformylation reaction in homogeneous systems.[1] The CO insertion reaction is the first step:

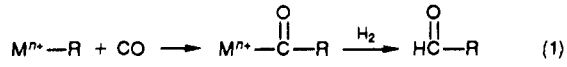

(1)

In general, the CO insertion proceeds under high pressure and the reverse reaction of decarbonylation of the acyl group takes place under vacuum.[1]

Recently, Asakura et al. reported a new aspect of reversible CO insertion on an SiO_2-attached Rh dimer catalyst which showed good catalytic activity for ethene hydroformylation.[2,3] Such heterogeneous catalysts were prepared by the reaction of *trans*-$[Rh(C_5Me_5)(CH_3)]_2(\mu\text{-}CH_2)_2$ with surface OH groups of SiO_2, with C_1 elimination as methane. FTIR spectroscopy showed that the CO insertion into an alkyl group to form acyl proceeds by heating the reaction to 423–473 K under vacuum, while the decarboxylation of the acyl group to form a dicarbonyl and an alkyl occurs under CO pressure at room temperature. On the basis of these findings and EXAFS bond length estimates, the following Scheme I was proposed. In it, the dotted line represents Rh–Rh bond cleavage. The CO pressure dependence observed for this reaction is opposite to that observed for Rh monomer catalysts, for which CO insertion into the metal–alkyl bond is brought about by CO pressure.[1] For the Rh dimer on silica, CO pressure decarbonylates the acyl. The fact that acyl formation was accompanied by Rh–Rh bond formation (2.70 Å bond length) led the authors of ref 2 to suggest that the insertion was in fact being promoted by the metal bond formation. There is little literature

Scheme I

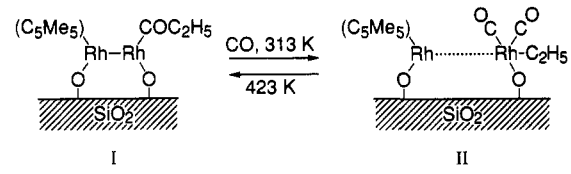

precedence for this idea. A homogeneous CO insertion involving Fe–Fe bond formation has been observed, but it is, unlike the above scheme, irreversible.[4,5]

The purpose of this paper is to undertake a theoretical examination of the electronic structure of species I and II and some potential reaction intermediates to understand the Rh–Rh bond cleavage in the above scheme. The proposed promotion effect of the metal bond formation on the acylation will be investigated.

Method and Models

We have substituted the silica support by hydroxyl groups and also substituted the C_5Me_5 ligand in Rh complexes by C_5H_5(Cp) to simplify the calculations. The choice of hydroxyl groups to represent the silica support is a simplifying approximation since the actual surface structures are not yet established. We have optimized the hydroxyl groups in our calculations because no surface structure information for SiO_2 is available for assigning surface oxygen spacing. We tried fixing the oxygen spacings to be 2.64 and 3.60 Å, respectively, based on spacings in (0001) planes of α-quartz. We found that the calculated structures experienced readjustments in bond angles and lengths and the energies became less stable by up to $^1/_2$ eV when the fixed oxygen spacings were used. Since we do not know what oxygen spacing we should use, we have begun by choosing the optimized ones.

(1) Evans, D.; Osborn, J. A.; Wilkinson, G. *J. Chem. Soc. A* **1968**, 3133.
(2) Asakura, K.; Kitamura-Bando, K.; Isobe, K.; Arakawa, H.; Iwasawa, Y. *J. Am. Chem. Soc.* **1990**, *112*, 3242.
(3) Kitamura-Bando, K.; Asakura, K.; Arakawa, H.; Sugi, Y.; Isobe, K.; Iwasawa, Y. *J. Chem. Soc., Chem. Commun.* **1990**, 253.
(4) Collman, J. P.; Rothrock, R. K.; Finke, R. G.; Rose-Munch, F. *J. Am. Chem. Soc.* **1977**, *99*, 7381.
(5) Collman, J. P.; Rothrock, R. K.; Finke, R. G.; Mooew, E. J.; Rose-Munch, F. *Inorg. Chem.* **1982**, *21*, 146.

0020-1669/92/1331-2651$03.00/0